14th Australasian Fluid Mechanics Conference
Adelaide University, Adelaide, Australia
10-14 December 2001

Shape Optimisation for Supersonic Nozzle Flows

D. H. Smith

DSTO/WSD, PO Box 1500, Salisbury SA, 5108 AUSTRALIA

Abstract

Constrained minimisation of the pressure integral in quasi one-dimensional nozzles is studied for supersonic inlet and subsonic exit conditions via active set methods with polynomial shape functions. Optimal configurations are generated and discussed in terms of geometry, shock location, constraints, boundary conditions and nonuniqueness.

Introduction

Shape optimisation in a flow context refers to choosing geometrical configurations in order to achieve optimal performance, as measured by a certain cost quantity. The essential elements of the process are a flow solver to compute flow solutions for given geometric parameters, and an optimiser to search for local minima of the cost function. For quasi one-dimensional nozzle flows, in which area ratio is the relevant geometrical quantity, optimisation was considered by Frank and Shubin[4], who performed velocity inversion with B-spline shape functions. This study will focus on the pressure integral along the nozzle, a quantity of theoretical numerical interest that serves as a useful computational model for lift and drag calculation. Pierce and Giles[9] consider this cost function from a numerical accuracy standpoint, demonstrating measures by which the accuracy is improved over that attained by the basic flow solver. The present study performs constrained minimisation and examines a number of associated numerical issues deemed to be important for later higher dimensional calculations.

First and second order accurate flow solutions are computed for low order polynomial shape functions via the Osher scheme[5] while a discrete adjoint gradient formulation with Gauss-Newton and DFP Hessian[3] updates enables quasi-Newton iteration on the cost function. The need for constraints quickly becomes apparent and these are imposed on the exit area, inlet slope and volume, with inequalities handled by an active set method. Iteration histories are monitored to observe the interplay between flow solver, optimiser, geometry and shock location, along with the key role played by constraints of various kinds. Studies of optimal shape behaviour with respect to boundary velocities see the emergence of multiple solutions.

Flow Governing Equations and Solution

The system of conservation equations governing steady quasi one-dimensional compressible flow in a variable area duct[4] can be reduced to the nonlinear ODE

$$\frac{d}{dx}\left(u+\frac{1}{u}\right)+\frac{A'}{A}\left(\frac{\gamma-1}{\gamma+1}u-\frac{1}{u}\right)=0 \qquad (1)$$

where $u(x)$ is the dimensionless velocity (Mach number here), $A(x)$ is the area ratio with $A(0)=1$, x is the normalised axial coordinate, $x\in[0,1]$, and γ is the ratio of specific heats. In smooth flow regions (1) can be integrated to give

$$uA\left[1-\theta u^2\right]^{\phi}=\text{constant}, \qquad (2)$$

where $\theta=\frac{\gamma-1}{\gamma+1}$ and $\phi=\frac{1}{\gamma-1}$, with solution branches in the (u,A) plane turning at sonic conditions, $u=1$. As A increases supersonic flow accelerates and subsonic flow decelerates. When a shock occurs (2) is applied in the smooth adjoining regions with the Rankine-Hugoniot jump conditions to yield three nonlinear equations for the left velocity u_l, shock area ratio A_s and right velocity u_r. For supersonic inlet conditions $u_0>1$, subsonic exit conditions $u_1<1$ and diverging geometry $A'(x)>0$ with exit area ratio A_1, unique single shock solutions obey

$$\begin{aligned} u_0\left(1-\theta u_0^2\right)^{\phi} &= u_l A_s\left(1-\theta u_l^2\right)^{\phi} \qquad (3)\\ u_l+\frac{1}{u_l} &= u_r+\frac{1}{u_r}\\ u_r A_s\left(1-\theta u_r^2\right)^{\phi} &= u_1 A_1\left(1-\theta u_1^2\right)^{\phi}, \end{aligned}$$

if the existence requirements on u_0, u_1 and A_1 are met[7]. Physically, these correspond to a region bounded by two limiting solutions, namely an inlet shock $A_s=1$ preceding entirely subsonic flow, and an exit shock $A_s=A_1$ preceded by entirely supersonic flow[4].

Discretisation and Numerical Solution

A numerical solution for the two point boundary value problem (1) with prescribed inlet and exit conditions is computed on a uniform spatial grid comprising N cells of width $h=\frac{1}{N}$, with discrete midcell velocity u_j defined at $x_j=(j-\frac{1}{2})h$. Integrating (1) over cell j and applying a midpoint rule for the source term gives

$$f_{j+1/2}-f_{j-1/2}+hg(u_j;A_j,A'_j)=0, \quad j=1,\ldots,N \qquad (4)$$

where the numerical flux function $f_{j+1/2}$ is derived from the Osher scheme with MUSCL extrapolation[5], producing a nonlinear system of algebraic equations for the vector of midcell velocities $\mathbf{u}$

$$\mathbf{f}(\mathbf{u}(\alpha),\alpha)=0, \qquad (5)$$

where α parametrises the geometry. Solutions are found with Newton iteration assisted by embedding[8] and Broyden Jacobian updates[1].

Nonuniqueness Behaviour

A linear diverging geometry $A(x)=1+cx$, with supersonic inlet and subsonic exit conditions admits unique solutions provided the necessary existence requirements are met[7]. If the area gradient $A'(x)$ is now allowed to vary by including a quadratic term, $A(x)=1+cx+bx(x-1)$, thus generating converging and diverging portions, then multiple solutions can appear. The familiar experimentally observed solution for this configuration comprises a shock in the diverging portion, with supersonic decelerating flow to the throat, acceleration to the shock and final subsonic deceleration to the exit. Embid et al[2] demonstrated the existence of a second unstable solution with shock in the converging section, in which the flow undergoes supersonic deceleration to the shock and subsonic acceleration to the throat before decelerating to the exit. Pseudo-arclength continuation[6] of the numerical solution (5) in the parameter b for fixed exit area ratio $A(1)=1.5$ and boundary velocities $(u_0,u_1)=(2.0,0.25)$ produces the branching diagram in Figure 1, confirming Embid's solution and revealing another un-

stable solution with two shock waves, one in the converging section and one in the diverging section.

Solving (3) for these conditions gives the shock area ratio $A_s = 0.795$, and inversion of the area ratio function gives two possible shock locations coinciding with stable and unstable single shock solutions for $b > 1.669$. Traversing the branch clockwise from point A sees shocks in the diverging section move upstream to the throat, at which the branch turns as the shock enters the converging section and loses stability. From here the postshock subsonic acceleration intensifies as b is increased, eventually becoming sonic and giving birth to a second shock in the diverging section. Solving (3) augmented with an equation enforcing sonic throat conditions gives the throat area ratio A^* at this transiton point, from which the corresponding $b = 2.59$. Both shocks then move downstream, governed by two sets of equations similar to (3), with the left shock weakening and collapsing to a sonic point at the turn. In this limiting solution the left shock area ratio equals the throat area to give $b = 4.12$. According to Embid it is possible to choose a geometry yielding arbitrarily many multiple solutions, of which the solutions demonstrated here represent a mere sample of the possibilities obtainable from higher order polynomial shapes.

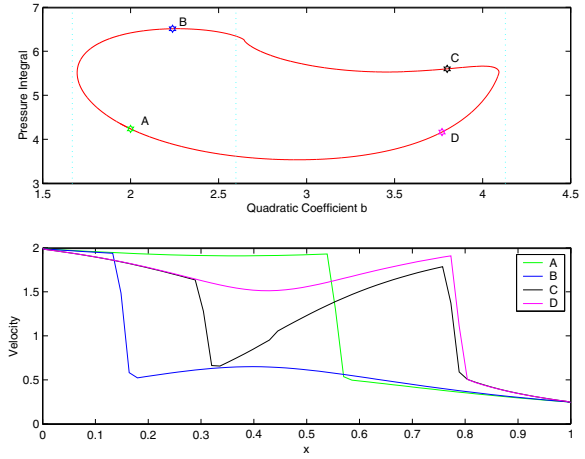

Figure 1: Branching of the numerical solution (5) for quadratic geometry at fixed exit area. Velocity profiles illustrate stable and unstable solutions with 1 or 2 shocks at A, B, C and D.

Shape Optimisation by Quasi-Newton Minimisation

The cost function under consideration here is the pressure integral along the nozzle, defined in terms of velocity by

$$\int_0^1 p(\alpha)\,dx = u_0 \int_0^1 \left[1 + \frac{\gamma-1}{2\gamma}(u_0^2 - u^2)\right] \frac{dx}{uA}, \qquad (6)$$

which is approximated by the midpoint rule

$$c(\alpha, \mathbf{u}(\alpha)) = hu_0 \sum_{j=1}^{N} \frac{1 + \frac{\gamma-1}{2\gamma}\left[u_0^2 - u_j(\alpha)^2\right]}{u_j(\alpha)A_j(\alpha)}, \qquad (7)$$

with accuracy depending on the flow solver. For a single shock solution (6) can be accurately evaluated by locating the shock from (3) and applying Romberg integration in the smooth regions upstream and downstream, $\int_0^1 p\,dx = \int_0^{x_s} p\,dx + \int_{x_s}^1 p\,dx$. Error estimates calculated on a series of spatial grids confirm first order accuracy from the first order flow solver and while the second order scheme offers considerable improvement, clean linear log error profiles are not achieved, with fitted exponents ranging from 1.7 to 2.7. Pierce and Giles utilise adjoint accuracy enhancement to achieve third order accuracy from the second order scheme[9], but do not perform optimisation. The cost function (7) will be minimised by quasi-Newton methods, which construct local quadratic approximations to $c(\alpha)$ from gradient and Hessian information. From the current iterate $\alpha^{(j)}$ a new iterate $\alpha^{(j+1)}$ is sought by line searching along the direction vector $\mathbf{p}^{(j)}$, which satisfies the linear system of equations

$$H(\alpha^{(j)})\mathbf{p}^{(j)} = -\nabla c(\alpha^{(j)}).$$

Discrete Adjoint Formulation

The cost function gradient for (7) is defined by

$$\nabla c(\alpha, \mathbf{u}(\alpha)) = \left(\frac{\partial A}{\partial \alpha}\right)^T \frac{\partial c}{\partial A} + \left(\frac{\partial \mathbf{u}}{\partial \alpha}\right)^T \frac{\partial c}{\partial \mathbf{u}}, \qquad (8)$$

where the terms $\frac{\partial A}{\partial \alpha}$, $\frac{\partial c}{\partial A}$ and $\frac{\partial c}{\partial \mathbf{u}}$ can be analytically evaluated. The flow derivative term $\frac{\partial \mathbf{u}}{\partial \alpha}$ can be calculated by solving the set of linear systems

$$\frac{\partial \mathbf{f}}{\partial \mathbf{u}}\frac{\partial \mathbf{u}}{\partial \alpha} + \frac{\partial \mathbf{f}}{\partial \alpha} = 0, \qquad (9)$$

derived by applying the implicit function theorem to the nonlinear flow equations (5), however a more efficient approach is to eliminate $\frac{\partial \mathbf{u}}{\partial \alpha}$ from (8) and (9) to give

$$\nabla c(A(\alpha), \mathbf{u}(\alpha)) = \left(\frac{\partial A}{\partial \alpha}\right)^T \frac{\partial c}{\partial A} + \left(\frac{\partial \mathbf{f}}{\partial \alpha}\right)^T \mu \qquad (10)$$

where the adjoint vector μ satisfies the linear system

$$\left(\frac{\partial \mathbf{f}}{\partial \mathbf{u}}\right)^T \mu + \frac{\partial c}{\partial \mathbf{u}} = 0. \qquad (11)$$

A Gauss-Newton type Hessian approximation[3] constructed from first derivative terms,

$$\begin{aligned}\frac{\partial^2 c}{\partial \alpha_l \partial \alpha_k} \approx hu_0 \frac{\gamma-1}{\gamma} \sum_j \left(\frac{2\gamma}{\gamma-1} + u_0^2\right) \frac{1}{u_j^3 A_j} \frac{\partial u_j}{\partial \alpha_l}\frac{\partial u_j}{\partial \alpha_k} \qquad (12)\\ + \left(\frac{\frac{2\gamma}{\gamma-1} + u_0^2}{u_j} - u_j\right) \frac{1}{A_j^3}\frac{\partial A_j}{\partial \alpha_k}\frac{\partial A_j}{\partial \alpha_l}\\ + \frac{1}{A_j^2 u_j^2}\left(\frac{\gamma}{\gamma-1} + \frac{u_0^2 + u_j^2}{2}\right)\left(\frac{\partial A_j}{\partial \alpha_l}\frac{\partial u_j}{\partial \alpha_k} + \frac{\partial A_j}{\partial \alpha_k}\frac{\partial u_j}{\partial \alpha_l}\right),\end{aligned}$$

provides a starting value from which subsequent DFP updates[3] are performed

$$H_{i+1}^{-1} = H_i^{-1} + \frac{\mathbf{z}\mathbf{z}^T}{\mathbf{z}^T\mathbf{y}} - \frac{H_i^{-1}\mathbf{y}\mathbf{y}^T H_i^{-1}}{\mathbf{y}^T H_i^{-1}\mathbf{y}},$$

where $\mathbf{z} = \alpha_{i+1} - \alpha_i$ and $\mathbf{y} = \nabla c_{i+1} - \nabla c_i$. Area ratio functions will take the polynomial form

$$A(x) = 1 + \alpha_1 x + \alpha_2 x(x-1) + \alpha_3 x(x-1)^2 + \alpha_4 x^2(x-1)^2.$$

Unconstrained Results

Unconstrained quadratic test calculations rapidly tend to pure diverging geometry, with successive iterations producing further growth accompanied by a drop in pressure on both sides of the shock, thus decreasing the cost function at the

expense of ever growing geometry. Similar behaviour occurs with cubic and quartic geometry, which produce diverging/converging/diverging shapes and develop a second shock from subsonic acceleration to sonic conditions in the converging section. From these tests it is readily apparent that constraints must be applied in order to achieve suitable convergence.

Linear Equality Constraints

Constraints of this type constitute the system $C^T\alpha = b$, where the columns of matrix C are the gradient vectors of the linear constraint functions, or normals of the constraint hyperplanes. At a local minimum α^* the absence of feasible descent directions demands that the gradient vector be expressible as a linear combination of the constraint normals, leading to the necessary condition $\nabla c(\alpha^*) = C\lambda^*$, where λ^* are the Lagrange multipliers. Generalised elimination methods[3] reduce the problem to one of unconstrained minimisation by effectively eliminating one variable for each constraint acting. The key element is a matrix Z whose columns are orthogonal to the constraint normals, $C^TZ = 0$, provided by a QR factorisation of C. Given a current feasible point $\alpha^{(j)}$ an arbitrary feasible point is expressed in terms of the reduced variables β, $\alpha = \alpha^{(j)} + Z\beta$, with associated cost function $c(\beta) = c(\alpha^{(j)} + Z\beta)$, gradient $\nabla_\beta c(\beta) = Z^T\nabla_\alpha c(\alpha)$ and Hessian $\nabla^2_\beta c(\beta) = Z^T\nabla^2_\alpha c(\alpha)Z$.

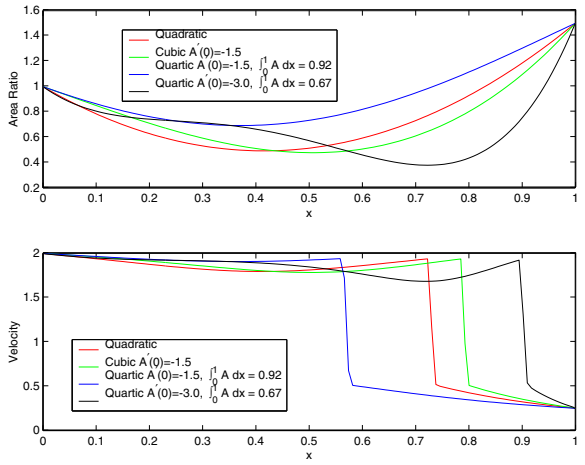

Figure 2: Equality constrained optimal nozzle shapes and velocity profiles for polynomial shape functions. Cost function values range from 2.62 to 4.21, and decrease as the shock moves downstream, shrinking the post-shock high pressure region.

To demonstrate the procedure first consider a quadratic nozzle with fixed exit area ratio $A(1) = 1.5$, or $\alpha_1 = 0.5$. For boundary velocities $(u_0, u_1) = (2.0, 0.25)$ and starting guess $\alpha^{(0)} = [0.5\ 2]^T$ the converged solution and corresponding velocity profile are shown in Figure 2 for a first order accurate flow solution on 128 flow cells. Repeating this calculation for cubic geometry produces divergence, however after also constraining the inlet slope $A'(0) = \alpha_1 - \alpha_2 + \alpha_3$ at its initial value of -1.5 a converged solution appears as shown. Compared to the quadratic case the nozzle throat is further downstream along with its shock while the inlet is less steeply inclined and the cost function is lower. A quartic calculation with the same constraints also diverges but after fixing the volume, $\int_0^1 A dx$, at its initial value gives a converged solution with shock well upstream of that for the previous two cases and higher cost function. A second quartic calculation starting from $\alpha^{(0)} = [0.5\ 3.5\ 0\ 0]^T$ with steeper converging inlet $A'(0) = -3$ and smaller volume produces a marked change in the optimal profile, pushing the shock further downstream to give the lowest cost function of the four cases. Upgrading these solutions to second order accuracy produces very little change to the final configuration, with slight cost reductions of less than 0.5% in each case.

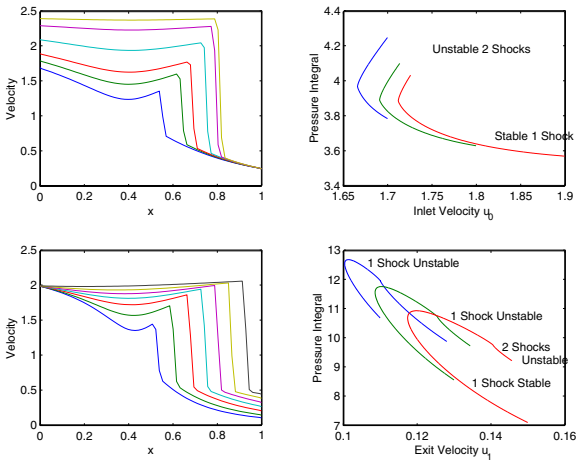

Figure 3: Behaviour of quadratic equality constrained solution with boundary velocity. The left plots display velocity profiles obtained by zero order continuation, which fail at limiting values of u_0 and u_1, and the right plots indicate flow solution behaviour near these points.

Varying the Boundary Conditions

In a practical situation the shape must be tuned to accomodate a range of inlet and exit conditions, prompting the obvious question of how the optimal solution depends on boundary conditions. Zero order continuation of the quadratic solution from Figure 2 with fixed exit area gives the series of velocity profiles in Figure 3, with each case meeting a lower limiting velocity at which continuation failure occurs. Freezing the geometry in the vicinity of these points and continuing the numerical flow solution in u_0 and u_1 by pseudo-arclength continuation[6] reveals turning points similar to those observed in Figure 1. For the inlet case the lower limit coincides with sonic throat conditions as seen at the right hand turning point of Figure 1. Decreasing the exit velocity u_1 at fixed u_0 sees the shock move upstream into the converging section, as in the the left hand turn of Figure 1, before a second shock is born from post shock subsonic acceleration becoming sonic. In both cases the unstable solutions incur higher cost functions than their stable counterparts so will not be attracted by the minimiser.

Inequality Constraints via Active Set Strategy

For inequality constrained minimisation, first order necessary Kuhn-Tucker conditions[3] at a local minimum stipulate that Lagrange multipliers of *active* constraints must be positive. Given a set of inequality constraints, active set methods[3] seek to fulfil these conditions by considering a sequence of equality constrained problems with associated active and inactive constraint sets. During the line search for a given EP, in which $\alpha(s) = \alpha^{(j)} + s\mathbf{p}^{(j)}$, the first inactive constraint violation defines a maximum allowable steplength s^*. If the computed steplength $s^{(j)}$ is too large it is reduced to s^* and the corresponding constraint is activated to give a new EP. Once a converged EP solution is attained the Lagrange multipliers are calculated for the active constraints via the previous QR decomposition and if these are all positive the necessary conditions are satisfied and

the process stops. Otherwise a feasible descent direction exists and the constraint with the most negative multiplier is removed from the active set to give a new EP.

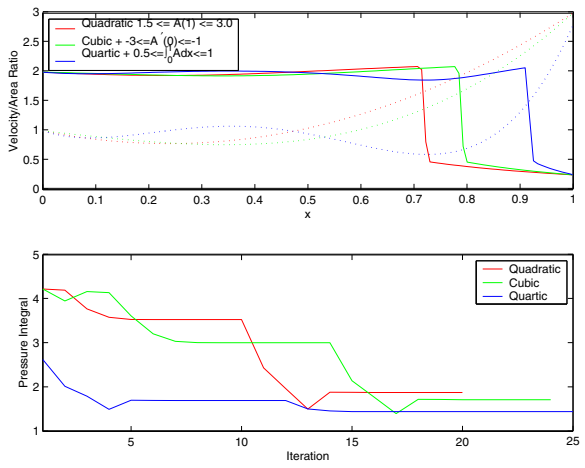

Figure 4: Inequality constrained minimisation results, with local minima in the cost function history showing inactive constraint violation and subsequent activation.

Return to the solutions displayed in Figure 2 and replace the equality constraints on the exit area, inlet slope and volume with corresponding bounds $1.5 \leq A(1) \leq 3$, $-3 \leq A'(0) \leq -1$ and $0.5 \leq \int_0^1 A\, dx \leq 1$. For the quadratic case with exit area bounds only the equality constrained solution at $\alpha_1 = 0.5$, or active lower bound, has a negative Lagrange multiplier indicating feasible descent by increasing α_1. The active set is thus emptied and subsequent unconstrained minimisation soon violates the upper bound $\alpha_1 = 2.0$, which is activated. Minimisation along this line converges to a local minimum with positive Lagrange multiplier, terminating the process. For the cubic case initial equality constrained iteration on $\alpha_1 = 0.5$ violates the upper inlet slope bound which then enters the active set. Equality constrained minimisation converges to a local minimum with negative Lagrange multiplier for the exit area lower bound, which after removal and further iteration sees violation of the upper exit area bound. Activating this and iterating then converges to a local minimum with two active constraints and positive Lagrange multipliers. Starting from the solution with $A'(0) = -3$ in Figure 2, with lower exit area and inlet slope bounds active, the quartic case initially violates the upper volume bound. Activating this and iterating then converges to a local minimum with negative Lagrange multiplier for the exit area lower bound, which is removed to give final convergence to a local minimum with two active constraints and the lowest cost function of all three cases. These results are summarised in Figure 4, where local minima in the cost function history indicate inactive constraint violation and activation.

One approach for handling nonlinear constraints is to apply the same methods within iterations on the nonlinear constraint functions. To demonstrate, reconsider the quadratic nozzle with additional bounds on the throat area, $A^* = 1 - \frac{(\alpha_1 - \alpha_2)^2}{4\alpha_2}$, chosen to accomodate the previous solution, $0.2 \leq A^* \leq 0.7$. Linearising and proceeding as before leads to several cycles in which the linearised upper A^* bound is violated, activated and then deactivated after linearising at the new iterate, before converging to become active. Iteration for this new EP then violates the upper exit area bound, which is activated while the newly linearised A^* bound becomes inactive. Final iteration along $\alpha_1 = 2.0$ arrives at the intersection point with both upper bounds active.

Conclusions

An active set method has been applied in conjunction with the discrete adjoint formulation and quasi-Newton iteration to minimise the pressure integral for quasi one-dimensional nozzles with supersonic inlet and subsonic exit conditions. Optimal configurations generated from polynomial shape functions favour downstream shock locations, and the the extra degrees of freedom afforded by higher order polynomials offer the lowest cost functions. Second order upgrades of first order accurate solutions show little difference, however this is not expected to be the case for higher dimensional calculations. Continuation studies in the boundary conditions indicate nonexistence regions, with turning points and unstable solutions emerging as the inlet or exit velocity is reduced to sufficiently small values. The calculations represent a basis for further study towards supersonic intakes.

Acknowledgements

The author is grateful to DSTO for granting leave and to JISTEC Japan for support while this work was conducted under an STA Fellowship Program at NAL Tokyo.

References

[1] C.G. Broyden, "A Class of Methods for Solving Nonlinear Simultaneous Equations", Math. Comp, **19** p577-593 (1965).

[2] P. Embid, J. Goodman and A. Majda, "Multiple Steady States for 1-D Transonic Flow", SIAM J. Sci. Stat. Comp. **5** 1 p21-41 (1984).

[3] R. Fletcher, *Practical Methods of Optimization*, Wiley (1987).

[4] P.D. Frank and G.R. Shubin, "A Comparison of Optimisation-Based Approaches for a Model Computational Aerodynamics Design Problem", J. Comp. Phys **98** 74-89 (1992).

[5] C. Hirsch, "Numerical Computation of Internal and External Flows", Wiley-Interscience (1990).

[6] H.B. Keller, "Numerical Solution of Bifurcation and Nonlinear Eigenvalue Problems", in Applications of Bifurcation Theory, edited by P.H. Rabinowitz, Academic NY (1977).

[7] Jens Lorenz, "Convergence of Upwind Schemes for a Stationary Shock", Math. Comp. **46** 173, p45-57 (1986).

[8] J.M. Ortega and W.C. Rheinboldt, Iterative Solution of Nonlinear Equations in Several Variables, Academic (1970).

[9] N. Pierce and M. Giles, "Adjoint Recovery of Superconvergent Functionals from PDE Approximations", SIAM Review **42** 2 p247-264 (2000).